Eur. Phys. J. B **31**, 53–61 (2003)
DOI: 10.1140/epjb/e2003-00008-8

THE EUROPEAN PHYSICAL JOURNAL B

Magnetic oscillations in the 2D network of compensated coupled orbits of the organic metal (BEDT-TTF)$_8$Hg$_4$Cl$_{12}$(C$_6$H$_5$Br)$_2$

D. Vignolles[1,2], A. Audouard[1,2,a], L. Brossard[1,2], S. Pesotskii[3], R. Lyubovskii[3], M. Nardone[1,2], E. Haanappel[2], and R. Lyubovskaya[3]

[1] Laboratoire de Physique de la Matière Condensée[b], 135 avenue de Rangueil, 31077 Toulouse, France
[2] Laboratoire National des Champs Magnétiques Pulsés[c], 143 avenue de Rangueil, 31432 Toulouse, France
[3] Institute of Problems of Chemical Physics, Russian Academy of Sciences, Chernogolovka 142432, Russia

Received 4 September 2002 / Received in final form 14 November 2002
Published online 27 January 2003 –

Abstract. Interlayer magnetoresistance and magnetisation of the quasi-two dimensional organic metal (BEDT-TTF)$_8$Hg$_4$Cl$_{12}$(C$_6$H$_5$Br)$_2$ have been investigated in pulsed magnetic fields extending up to 60 T and 33 T, respectively. About fifteen fundamental frequencies, composed of linear combinations of only three basic frequencies, are observed in the oscillatory spectra of the magnetoresistance. The dependencies of the oscillation amplitude on the temperature and on the magnitude and orientation of the magnetic field are analyzed in the framework of the conventional two-dimensional Lifshitz-Kosevitch (LK) model. This model is implemented by damping factors which accounts for the magnetic breakthrough occurring between electron and hole orbits yielding conventional Shubnikov-de Haas closed orbits (model of Falicov and Stachowiak) and quantum interferometers. In particular, a quantum interferometer enclosing an area equal to the first Brillouin zone area is evidenced. The LK model consistently accounts for the temperature and magnetic field dependence of the oscillation amplitude of this interferometer. On the contrary, although this model formally accounts for almost all of the observed oscillatory components, it fails to give consistent quantitative data in most other cases.

PACS. 71.18.+y Fermi surface: calculations and measurements; effective mass, g factor – 71.20.Rv Polymers and organic compounds – 72.20.My Galvanomagnetic and other magnetotransport effects

1 Introduction

The model of a linear chain of coupled orbits, considered at the time as purely academic, was introduced by Pippard [1] in the early sixties to compute magnetic breakthrough (MB)-induced Shubnikov-de Haas (SdH) and de Haas-van Alphen (dHvA) oscillations. This model has received a spectacular illustration with the BEDT-TTF (bisethylenedithia-tetrathiofulvalene) salts of the κ-family. Magnetic oscillations have been extensively studied especially in κ-(BEDT-TTF)$_2$Cu(SCN)$_2$ for which, in addition to the basic frequencies associated with the closed α and the MB-induced β orbit (F_α and F_β, respectively) magnetoresistance and magnetisation oscillation spectra exhibit frequencies which are combinations of F_β and F_α. On the basis of the Falicov and Stachowiak model [2], which assumes highly degenerate sharp Landau levels, these oscillations have been interpreted either on the basis of conventional SdH or dHvA effect (*e.g.* $F_\beta+F_\alpha$ or $F_\beta + 2F_\alpha$ [3–5]) or quantum interference (QI) (*e.g.* $F_\beta - F_\alpha$ [4,5] or $F_\beta - 2F_\alpha$ [5]). However, these latter frequencies are also observed in dHvA data [3,6,7], although dHvA oscillations are not sensitive to QI. It has been computed that oscillation of the chemical potential of a 2D-electron gas [4,8] may account, at least partly, for the frequency mixing observed in dHvA spectra. Nevertheless, numerical [9] and analytical [10] calculations of the dHvA oscillations for the Fermi surface (FS) of κ-salts indicate that significant frequency mixing can also be obtained within the grand canonical ensemble *i.e.* for a fixed chemical potential. More generally, as already pointed out for the case of pure magnesium [11], the coupled-orbit network model of Pippard [1], which is characterised by

[a] e-mail: audouard@insa-tlse.fr
[b] UMR 5830: Unité Mixte de Recherche CNRS – Université Paul Sabatier – INSA de Toulouse
[c] UMS 5642: Unité Mixte de Service CNRS – Université Paul Sabatier – INSA de Toulouse

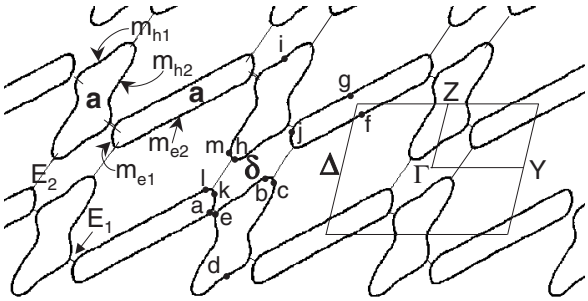

Fig. 1. Fermi surface of $(BEDT\text{-}TTF)_8Hg_4Cl_{12}(C_6H_5Cl)_2$ according to band structure calculations of Vieros *et al.* [14]. In addition to the elongated electron and the hole closed orbits (a orbits), the δ and Δ pieces are indicated. m_{e1} (m_{h1}) and m_{e2} (m_{h2}) are the weight factors, *i.e.* the partial effective masses linked to the short and long parts of the electron (hole) closed orbits, respectively. E_1 and E_2 are the gaps which separate the electron and hole orbits. Other Latin labels are discussed in the text.

a magnetic band structure with broadened Landau levels, may be a better basis to account for the so-called forbidden frequencies [10,12]. Unfortunately, no such quantitative model for the magnetoresistance oscillations at finite temperature in a network of coupled orbits is, to our knowledge, available in the literature.

Another type of network of coupled orbits is provided by the isostructural organic compounds of the family $(BEDT\text{-}TTF)_8Hg_4X_{12}(C_6H_5Y)_2$ where X, Y = Cl, Br. Among these compounds, those with X = Cl exhibit a metallic character down to the lowest temperature [13]. Their room temperature FS has been calculated for X, Y = Cl [14], which is referred hereafter to as the (Cl, Cl) compound. It results from the hybridization of two pairs of quasi-1D sheets parallel to the a^*c- and $a^*(b+c)$-plane, respectively [13,14], which leads to one hole and one elongated electron tube (see Fig. 1). The cross section area of the compensated electron and hole tubes amounts to about 13 percent of the first Brillouin zone (FBZ) area [14]. Nevertheless, the corresponding orbits do not share the same topology and are separated from each other by two unequal gaps labelled E_1 and E_2 in Figure 1. Provided these gaps are not too large in view of the strength of the magnetic field, this FS gives rise to a two-dimensional (2D) network of quasi-2D compensated orbits rather than a linear chain of coupled orbits as in the case of the κ-(BEDT-TTF) salts. One of the consequences offered by such a FS topology is, as developed below, that no forbidden frequency can be defined in (Cl, Cl). Magnetoresistance data recorded up to 36 T in this compound [15] have revealed a very complex oscillatory spectrum consisting of linear combinations of the three basic frequencies F_a, F_δ and F_Δ, which are respectively linked to the compensated closed electron and hole orbits (a orbits) and to the FS pieces δ and Δ located in between (see Fig. 1). In particular, the frequency $F_b = 2F_a + F_\delta + F_\Delta$, which corresponds to the area of the room temperature FBZ, has been observed. Although the data analysis, performed in the framework of the Falicov-Stachowiak model, has revealed that frequencies F_a and $F_{2a+\delta}$, on the one hand, and $F_{a+\delta}$ and F_b, on the other hand, are compatible with the SdH effect and QI, respectively, it has been suggested that other contributions may significantly contribute to the oscillatory behaviour.

The aim of this paper is to provide further insight on this topic. For this purpose, interlayer magnetoresistance and dHvA oscillations of the $(BEDT\text{-}TTF)_8Hg_4Cl_{12}(C_6H_5Br)_2$, referred to hereafter as the (Cl, Br) compound are reported. An even better signal-to-noise ratio than for the previous magnetoresistance measurements on the (Cl, Cl) compound has been achieved. This allows, on the basis of the Falicov-Stachowiak and QI models, more extensive analysis of the oscillatory data than that performed on the (Cl, Cl) compound.

2 Experimental

The studied crystal was a platelet with approximate dimensions $(1\times1\times0.1)$ mm^3, the largest sides being parallel to the conducting bc-plane. Magnetoresistance measurements were performed in pulsed magnetic field either up to 60 T (pulse decay duration 0.18 s) and in the temperature range from 0.28 K to 5 K (see Ref. [16] for experimental details on the ^{3}He cryostat used in the experiments) or up to 36 T (pulse decay duration 1 s) in the temperature range from 1.6 K to 13 K. In the first case, the field direction was at $\theta = 11°$ from the normal to the conducting bc-plane (the sign of θ is arbitrary). In the second case, a rotating sample holder allowed to change the direction of the magnetic field with respect to the conducting plane. Electrical contacts were made to the crystal using annealed gold wires of 20 μm in diameter glued with graphite paste. Alternating current (400 μA, 50 kHz) was injected parallel to the a^* direction (interlayer configuration). A lock-in amplifier with a time constant of 30 μs and 100 μs for 60 T pulses and 36 T pulses, respectively was used to detect the signal across the potential leads. Magnetisation was measured by the cantilever method [17] during 33 T pulses (pulse decay duration 1 s) in the torque mode configuration for which the signal is proportional to $M_\parallel B\tan(\theta)$, where $M_\parallel$ is the component of the magnetisation parallel to B. Therefore, the sensitivity of the magnetisation measurements increases as the magnetic field increases. Due to the limited resonance frequency of the cantilever ($f_{res} = 500$ Hz), reliable data can only be obtained for oscillation frequencies lower than *e.g.* $F = 1500$ T at $B = 30$ T.

3 Results and discussion

Examples of field-dependent interlayer resistance and magnetisation, measured in pulsed magnetic field of up to 60 T and 33 T, respectively, are displayed in Figure 2. A rough value of the sample magnetisation is 1 A/m at 33 T. In the following, the frequencies involved in the oscillatory

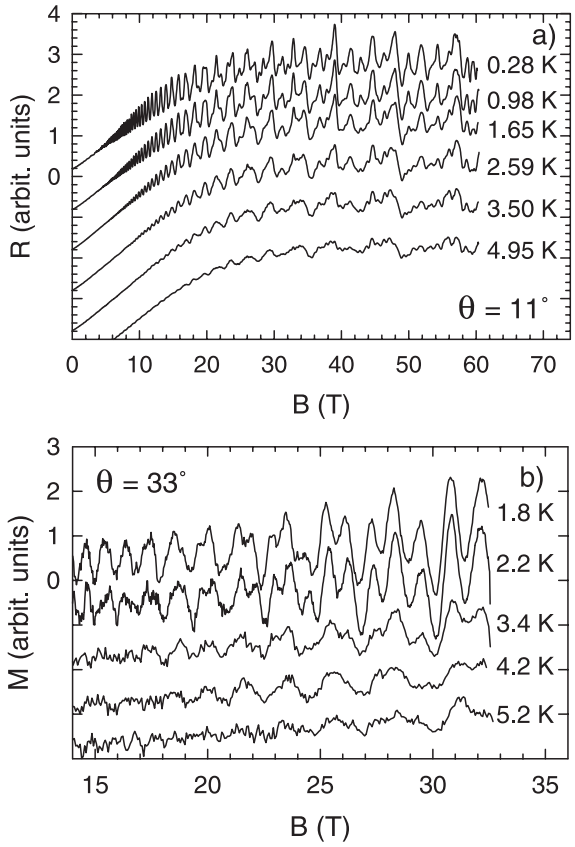

Fig. 2. Interlayer magnetoresistance (Fig. 2a) and magnetisation (Fig. 2b) data. The curves are shifted from each other by 1 in Figures 2a and b.

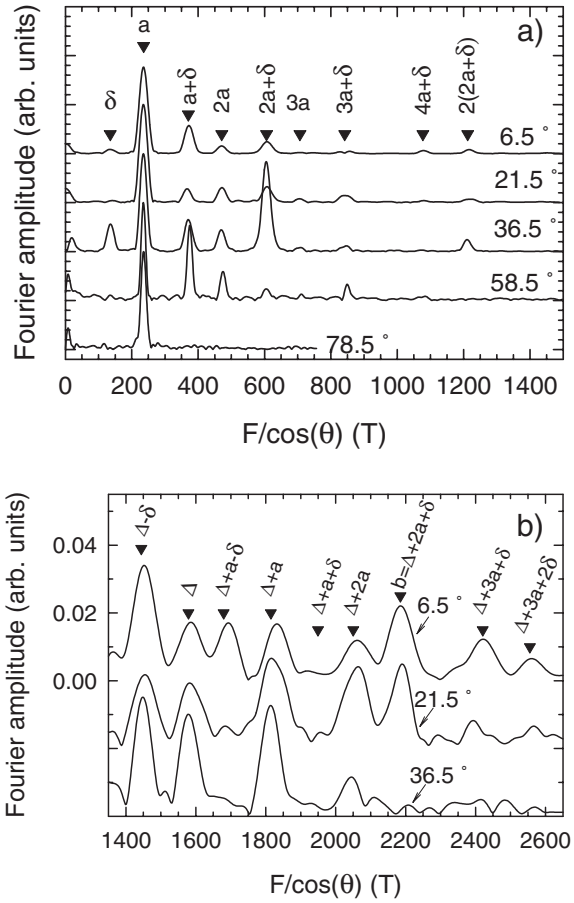

Fig. 3. Fourier transforms deduced from magnetoresistance data at 1.8 K for different orientations of the magnetic field. The magnetic field window is 10–30 T and 18–36 T for Figures 3a and b, respectively. θ is the angle between the magnetic field direction and the normal to the conducting plane. Data are normalised to the amplitude of the a oscillations (this masks the actual θ dependence of the oscillations amplitude, the study of which is outside the scope of the paper). Down triangles are marks calculated with $F_\delta = 135$ T, $F_a = 235.5$ T and $F_\Delta = 1579$ T.

spectra of such data are first determined and considered in connection with the calculated FS (see Sect. 3.1). Calculations, on the basis of the semiclassical model of coupled orbits [2] and the QI model [18,19], of the effective masses and of the damping factors relevant to the oscillations evidenced in Section 3.1 are reported in Section 3.2. Finally, the dependencies of the oscillations amplitude on the temperature and on the magnitude and orientation of the magnetic field are studied (in Sects. 3.3 and 3.4, respectively) in the framework of the LK model in order to check to what extent conventional SdH effect and QI phenomenon are able to give a consistent picture of the oscillatory data.

3.1 Oscillatory spectrum

The main feature of the oscillatory spectrum is the large number of fundamental frequencies that are observed in the Fourier transform (FT) of the oscillatory magnetoresistance (see Fig. 3). These frequencies exhibit a clear 2D behaviour as the direction of the magnetic field is varied with respect to the normal to the conducting plane. The frequency values given below take into account the data collected for θ ranging from $-49°$ to $78.5°$. The oscillations with frequency $F_a = (235.5 \pm 1.0)$ T have the highest amplitude at 1.8 K. As for the (Cl, Cl) compound [15] and in agreement with band structure calculations, they can be attributed to the closed electron and hole orbits, while the oscillations with frequency $F_\delta = (135.0 \pm 1.5)$ T are attributed to the FS piece labelled δ in Figure 1. The frequency $F_b = (2185 \pm 20)$ T (see Fig. 3b), which corresponds to $(100 \pm 1)\%$ of the room temperature FBZ area of (Cl, Br) is equal to $2F_a + F_\Delta + F_\delta$. This yields $F_\Delta = (1579 \pm 24)$ T, in agreement with data in Figure 3b where an oscillation with frequency (1577 ± 20) T can be noticed. As in the case of (Cl, Cl), all the frequencies observed in Figure 3 are linear combinations of the 3 basic frequencies F_a, F_δ and F_Δ with cross sections $(10.8 \pm 0.1)\%$, $(6.2 \pm 0.1)\%$ and $(72.3 \pm 0.9)\%$ of the FBZ area, respectively. Quite good agreement, close to

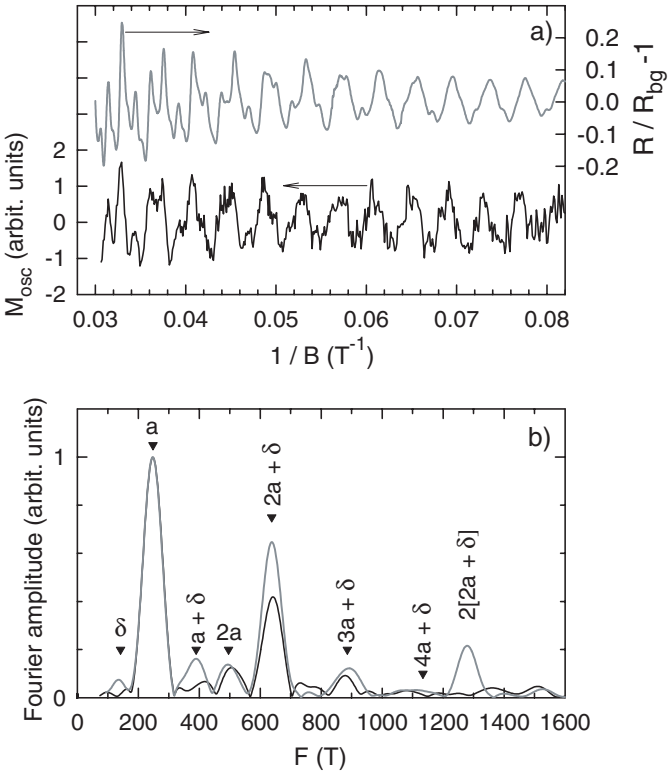

Fig. 4. Oscillatory part of the magnetoresistance (R_{bg} is the background part) and of the magnetisation at $\theta = 17°$ and $T = 1.8$ K (a). The corresponding Fourier transforms are displayed in (b). Grey and black trace corresponds to magnetoresistance and magnetisation data, respectively.

one percent, with the FS pieces labelled a, δ and Δ in Figure 1, relevant to the (Cl, Cl) compound, and with the data in reference [15] is observed. It is worthwhile to notice that a commensurability relationship is observed between the basic frequencies. Indeed, $5F_a+3F_\delta = (1582.5\pm9.5)$ T which is equal to F_Δ within error bars. Nevertheless, $5a + 3\delta$ oscillations correspond to SdH orbit or QI path with much larger effective mass and reduced value of R_{MB} (see Sect. 3.2) when compared to Δ oscillations and are not considered in the following.

The frequencies F_a and $F_{2a+\delta}$ are clearly observed in the dHvA data (see Fig. 4). Nevertheless, if F_δ seems to be absent from the dHvA spectra, the signal-to-noise ratio is not large enough to decide whether frequency combinations such as $F_{a+\delta}$ and $F_{3a+\delta}$ are present or not. As a consequence, reliable data can only be derived from the magnetisation data for the a and the $2a+\delta$ series.

3.2 Calculation of effective masses and damping factors

The amplitude of a given oscillation series is conventionally given by the product of the thermal (R_T),

Table 1. Calculated effective mass (m*) and field-dependent part of the MB damping factor (R_{MB}, see Eq. (3)) relevant to the observed oscillation series. Δ_i stands for $|m_{ei} - m_{hi}|/m^*(a)$ (see Fig. 1). For a given oscillation, only the SdH orbits and QI paths yielding the lowest effective mass and the highest value of the MB damping factor are considered in the table.

	$m^*/m^*(a)$		R_{MB}	
	SdH	QI	SdH	QI
δ and Δ	4	2	$q_1^6q_2^6p_1^2p_2^2$	$q_1^4q_2^4p_1^2p_2^2$
a	1		$q_1^2q_2^2$	
$a+\delta$	3	1	$q_1^4q_2^4p_1^2p_2^2$	$q_1^2q_2^2p_1^2p_2^2$
$2a+\delta$	2	$2\Delta_2$	$q_1^2q_2^2p_1^2p_2^2$	$q_1^4q_2^2p_1^2p_2^2$ or $q_1^2q_2^4p_1^2p_2^2$
$3a+\delta$	3	1	$q_1^4q_2^4p_1^2p_2^2$	$q_1^4q_2^4p_1^2p_2^2$
$4a+\delta$	4	$[4\Delta_2+2\Delta_1]$	$q_1^6q_2^6p_1^2p_2^2$	$q_1^6q_2^6p_1^2p_2^2$
b	4	0	$q_1^2q_2^6p_1^6p_2^2$ or $q_1^6q_2^2p_1^2p_2^6$	$q_1^4p_1^2p_2^4$ or $q_2^4p_1^4p_2^2$

Dingle (R_D), MB (R_{MB}) and spin (R_s) damping factors:

$$R_T \propto Tm_c/B\sinh(u_0Tm_c/B) \quad (1)$$

$$R_D = \exp(-u_0T_Dm_c/B) \quad (2)$$

$$R_{MB} \propto \prod_{g=1,2} p_g^{n_{pg}} q_g^{n_{qg}} \quad (3)$$

$$R_s = \cos\mid \pi g^* m_c(\theta=0)/2\cos\theta \mid \quad (4)$$

where $u_0 = 14.694$ TK^{-1}. T_D, m_c and g^* are the Dingle temperature, the cyclotron effective mass and the effective Landé factor, respectively. Equation (1) holds for 2D FS. Equation (3) only takes into account the field-dependent part of R_{MB}. The index g stands for the two different gaps E_1 and E_2 between electron and hole orbits (see Fig. 1). The integers n_{pg} and n_{qg} are respectively the number of tunnelling and Bragg reflections encountered along the path of the quasiparticle. The tunnel and Bragg reflection probability amplitudes are given by $p_g^2 = \exp(-B_g/B)$, where B_g is the MB field, and $p_g^2 + q_g^2 = 1$. The field-dependent part of the MB damping factor relevant to the various oscillations considered in the following, are given in Table 1 for SdH orbits and QI paths.

According to Falicov and Stachowiak [2], the effective mass linked to a given conventional SdH orbit can be expressed as the sum of weight factors, which can be regarded as absolute values of partial cyclotron masses of FS pieces. This assumption accounts for the MB orbits of 3D metals such as Mg [2,20]. Nevertheless, contrary to the case of κ-salts or Mg, the FS of the (Cl, Cl) and (Cl, Br) compounds is strongly asymmetrical so that the effective masses linked to electron and hole orbits, expressed as $m_e^* = 2(m_{e1} + m_{e2})$ and $m_h^* = 2(m_{h1} + m_{h2})$, respectively (see Fig. 1), may be different. Since the oscillations with frequency F_a result from the contribution of these two orbits, the resultant effective cyclotron mass is approximated in the following by $m_a^* = (m_e^* + m_h^*)/2$, *i.e.*

$m_a^* = m_{e1} + m_{e2} + m_{h1} + m_{h2}$. The same type of calculation is performed for the other SdH orbits reported in Table 1. It should nevertheless be noticed that this statement is only valid provided m_e^* and m_h^* are close to each other. If not, only the orbit with the lowest effective mass significantly contributes to the considered oscillation amplitude. In the framework of the QI model [18,19], the effective mass relevant to a given interferometer is given by the difference between the effective masses m_i^* and m_j^* of its two arms i and j: $m^* = \mid m_i^* - m_j^* \mid$. It should be kept in mind that a given oscillation series can be accounted for by several types of QI paths or SdH orbits with different damping factors, as discussed in [15]. Data in Table 1 is restricted to orbits and paths yielding the highest value of the damping factors *i.e.* with the lowest number of MB junctions and the lowest effective mass.

Following Falicov and Stachowiak [2] and Shoenberg [20], areas enclosed by electron and hole closed orbit have opposite signs. The a, $2a + \delta$ and $2a + \Delta$ orbits may have either electron or hole character and thus different sign. Any linear combination of the frequencies linked to these three orbits can then be observed within the semiclassical picture, provided the value of the relevant damping factors is not too small. As a consequence, contrary to the case of the linear chain of coupled orbits, there is no forbidden orbit in such a 2D network of coupled compensated orbits. In particular, very large SdH orbits and QI paths including both electron and hole parts may account for a given (even rather low) frequency, although with a reduced value of the damping factor and a large effective mass. This is the case of F_δ which can be attributed, among others, to both the semiclassical MB closed orbit (a b c d e b f g h m i h l a) and the QI path (a k l)-(a b c d e b f g h l) (see Fig. 1). In that respect, it can be remarked that, although F_δ and F_Δ are significantly different, their effective mass and MB damping factor are identical.

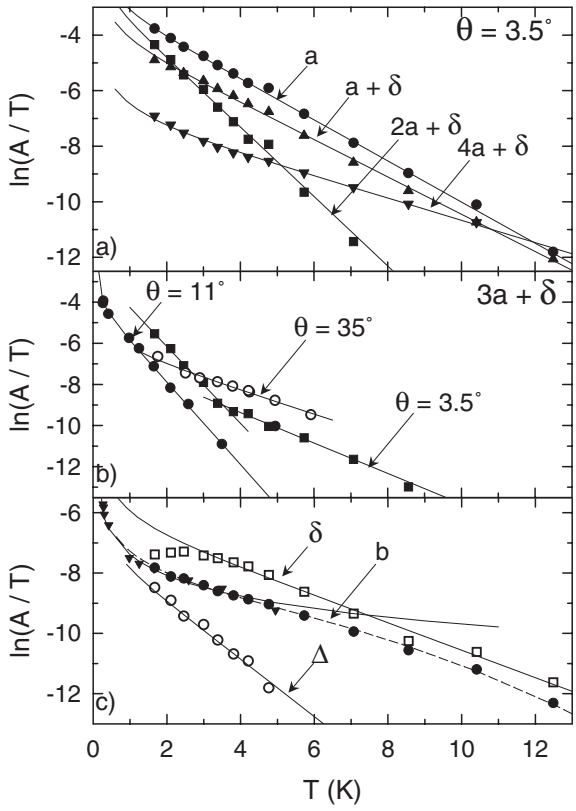

Fig. 5. Temperature dependence of the oscillation amplitude (A) of some of the series observed in Figure 3. The magnetic field window of the Fourier transform is 11.4 T–35.7 T and 23 T–35.7 T for δ and b oscillations, respectively. For all the other oscillations, the magnetic field window is 18 T–35.7 T. Data for δ and Δ are at $\theta = 3.5°$; data for b are at either $\theta = 3.5°$ (solid circles) or at $\theta = 11°$ (down triangles). Solid lines are best fits to equation (1). For b oscillations, a zero effective mass is assumed. The dashed line takes into account a temperature-dependent quantum lifetime (see text and Refs. [15,21]).

3.3 Experimental cyclotron effective mass parameter

Conventional plots of the temperature dependence of the amplitude of some of the magnetoresistance oscillation series are displayed in Figure 5. It has been checked that the cyclotron effective mass parameters (m_c) follow the $1/\cos(\theta)$ law expected for a 2D FS and that dHvA and magnetoresistance data yield consistent results for the a and $2a + \delta$ oscillations. However, a few unusual features, not predicted by the LK model, are observed: the kink in the temperature dependence of the amplitude of $3a+\delta$ (see Fig. 5b) and the downward deviation from the LK model at low temperature for the δ oscillations (see Fig. 5c). In most cases, a good agreement with the LK model (Eq. (1)) is nevertheless observed (see solid lines in Fig. 5).

The deduced cyclotron effective mass parameters, are given in Table 2 and compared to the data for (Cl, Cl). Similar values are obtained for both compounds. Assuming the a oscillations result from the conventional SdH effect, the comparison between the experimental data for $m_c/m_c(a)$ and the calculated values of $m^*/m^*(a)$ allows

Table 2. Experimental cyclotron effective masses (m_c) for the (Cl, Cl) [15] and (Cl, Br) compounds. $^\natural$ data for b oscillation are compatible with a zero effective mass at low temperature and in a large temperature range by assuming a temperature-dependent quantum lifetime (see Refs. [15,21] and the dashed line in Fig. 5c).

	Cl-compound	Br-compound	
	m_c	m_c	$m_c/m_c(a)$
δ	0.50±0.15	0.45±0.10	0.39±0.12
a	1.17±0.13	1.15±0.10	1
$a + \delta$	1.02±0.08	1.00±0.07	0.87±0.14
$2a + \delta$	1.95±0.10	2.10±0.16	1.83±0.30
$3a + \delta$ (high T)	0.73±0.15	0.72±0.06	0.63±0.11
$3a + \delta$ (low T)		2.95±0.20	2.57±0.40
$4a + \delta$		0.35±0.07	0.30±0.09
Δ		1.15±0.15	1.00±0.22
b	$0^\natural$	$0^\natural$	$0^\natural$

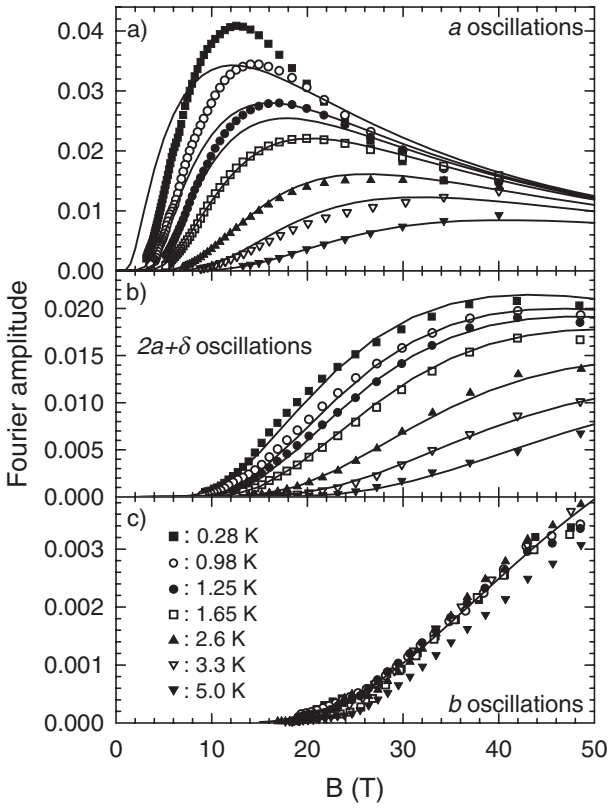

Fig. 6. Magnetic field dependence of the amplitude of the a (Fig. 6a), $2a + \delta$ (Fig. 6b) and b (Fig. 6c) oscillations. Solid lines in Figures 6a and b are best fits of equations (1) to (3) to the data with $B_0 = 33$ T [23]. Solid line in Figure 6c is obtained with $B_0 = 45$ T (see text).

us to determine the SdH orbits or QI paths that are compatible with a given oscillation series [15]. In that respect, the amplitude of the b oscillations has been found to be roughly temperature-independent up to ∼4.5 K (see Fig. 6c) which is consistent with a zero cyclotron effective mass and compatible with QI only (see Tab. 1). A strong downward deviation from the LK model is nevertheless observed in the higher temperature range for these oscillations (see Fig. 5c). Such a behaviour has already been observed for the 3D metal LaB_6 [21] and the (Cl, Cl) compound [15] and attributed to the temperature dependence of the quantum lifetime (see dashed line in Fig. 5c).

In summary, according to the temperature dependence of the oscillations amplitude, data for $3a + \delta$ in the low temperature range and $2a + \delta$ series are compatible with conventional SdH effect; data for $a + \delta$, $4a + \delta$ (provided $\mid m_{e1} - m_{h1} \mid$ and $\mid m_{e2} - m_{h2} \mid$ are small enough) and b are consistent with QI; data for $3a + \delta$ in the high temperature range, δ and Δ cannot be accounted for by neither SdH effect nor QI.

Before checking these provisional inferences, in Section 3.4, it is interesting to remark that, in addition to the b oscillations, few others bear small effective cyclotron mass parameter. This is the case of the δ and $4a + \delta$ oscillations (see Tab. 1) the amplitude of which remains high enough to be observed directly on the magnetoresistance data at high temperature, as evidenced in Figure 7.

3.4 Magnetic field dependence of the oscillation amplitude

In the following, the dependence of the amplitude of the magnetoresistance oscillations on the magnitude and orientation of the magnetic field is investigated at 1.8 K. DHvA measurements are not considered since reliable data were obtained in a narrow magnetic field range only. Similarly, the $3a + \delta$ oscillation is also not analyzed since this series does not follow the LK behaviour.

In the low field limit, equations (1–4) reduce to:

$$A \propto B^{-1} \exp(-\alpha/B) \tag{5}$$

where A is the oscillation amplitude and $\alpha = u_0(T + T_D)m_c + (n_{p1}B_1 + n_{p2}B_2)/2$. Since the a oscillation only involves Bragg reflections, α further reduces to $u_0(T + T_D)m_c$ which allows us to determine T_D from the low field slope α of the so-called Dingle plots in this case. A Dingle temperature $T_D = (0.2 \pm 0.2)$ K is extracted from the α values reported in Figure 8, which is the signature of a very good crystal. Similarly, it is easy to check that the most pronounced damping of the oscillation amplitude as the magnetic field increases is observed in the case of the a series. This feature allows us to determine the MB field as accurately as possible from the field dependence of the amplitude of the oscillations of this series. Nevertheless, since the MB gaps E_1 and E_2 are different according to band structure calculations (see Fig. 1), only an average value B_0 of B_1 and B_2, without any real physical sense, can be derived from the data [22]. The inset of Figure 8 displays the magnetic field dependence of the amplitude of the a oscillations for some directions of the magnetic field. Black and grey lines are best fits of equations (1–4) and (5) to the data, respectively. The angle dependence of B_0 and α deduced from such data are displayed in Figure 8. Even though α nicely follows the $1/\cos(\theta)$ law expected for a 2D FS, B_0 exhibits a strongly non-monotonic angle dependence. As an example, while no MB is required, at least up to 30 T, to account for the data at $\theta = -23.5°$, strong MB-induced damping of the amplitude is observed at $\theta = -5.5°$ (see inset of Fig. 8). The mean MB field at $\theta = 0°$ is $B_0(0°) = (35 \pm 7)$ T which is to be compared to the MB field of the (Cl, Cl) compound ($B_0(0°) = (55 \pm 20)$ T).

It can be seen in Table 1 that for $a + \delta$ (QI), $2a + \delta$ (SdH) and $4a + \delta$ (QI), n_{p1} and n_{p2} are both equal to 2. For these oscillations, the low field slope of the Dingle plots is $\alpha = u_0(T + T_D)m_c + 2B_0$. On the whole, α follows a $1/\cos(\theta)$ law for these oscillations (see solid lines in Fig. 9), as it is the case for the a oscillations. Some deviations are nevertheless observed, for the $a + \delta$ and $4a + \delta$ oscillations only, which might qualitatively account for the non-monotonic angle dependence of B_0 derived

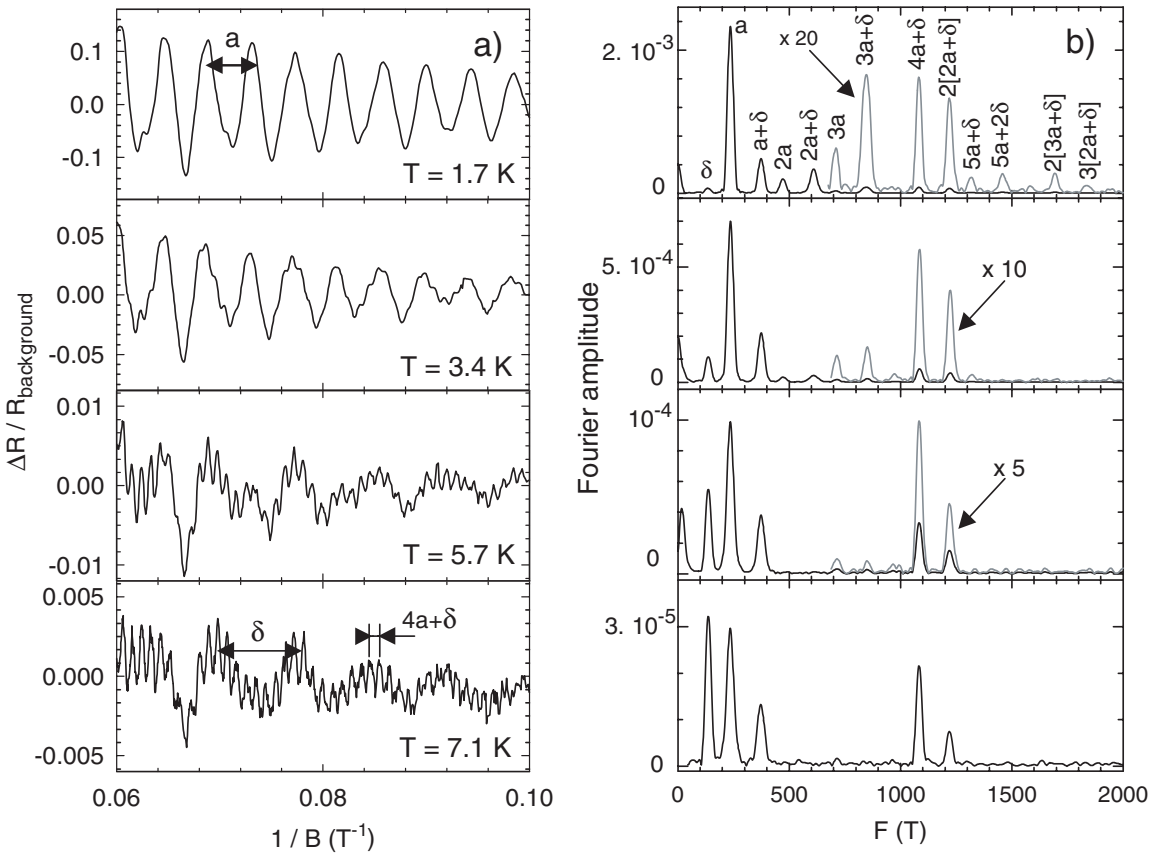

Fig. 7. Oscillatory part of the magnetoresistance at different temperatures (a) and corresponding Fourier transforms (b). The angle between the magnetic field direction and the normal to the conducting plane is $\theta = 3.5°$.

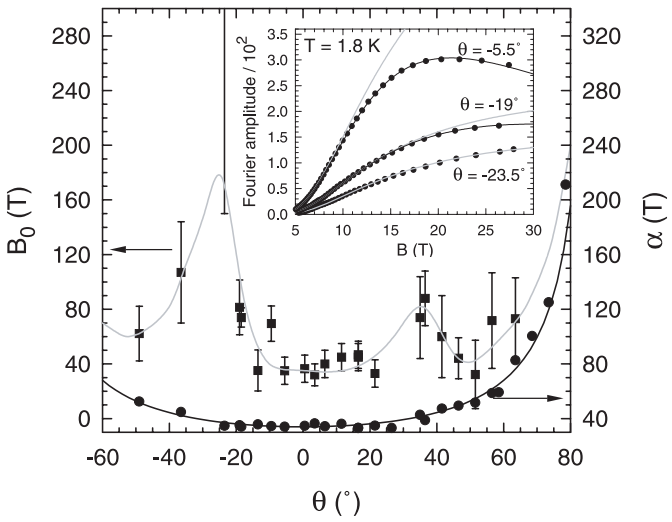

Fig. 8. Angle (θ) dependence of the MB field (B_0) and of the slope of the Dingle plots at low magnetic field (α, see Eq. (5)) of the a series at $T = 1.8$ K. The black line is the best fit of the $1/\cos(\theta)$ law to the data with $\alpha(\theta = 0°) = 34$ T. The grey line is a guide to the eye. The inset displays the field dependence of the a oscillations amplitude for some directions of the magnetic field. Black and grey lines are best fits of equations (1–4) and (5) to the data, respectively.

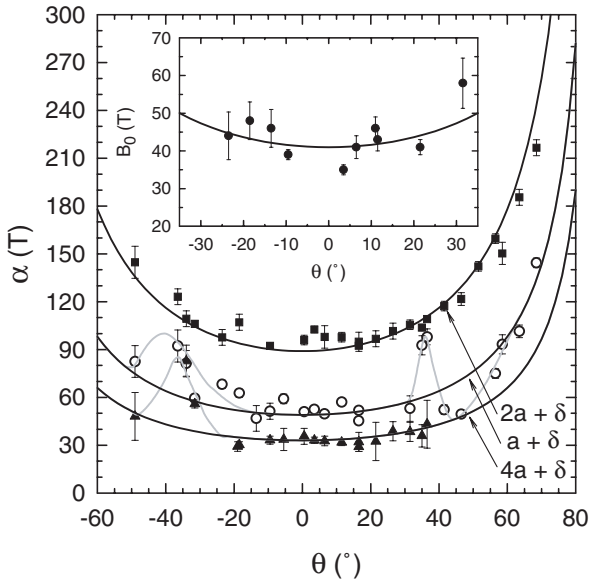

Fig. 9. Angle (θ) dependence of the slope of the Dingle plots at low magnetic field (α) at $T = 1.8$ K for the $a+\delta$, $2a+\delta$ and $4a+\delta$ series. The inset displays the MB field values deduced from data for b oscillations. Black lines are best fits of the $1/\cos(\theta)$ law to the data. Grey lines are guides to the eye.

from the a oscillations (Fig. 8) if they were observed also for the $2a+\delta$ oscillations (which is not the case). Be that as it may, owing to the $B_0(\theta = 0°)$ value deduced from Figure 8 and the effective cyclotron mass values reported in Table 2, the values of α reported in Figure 9 are too small in order to account for the SdH orbits or QI paths inferred from the temperature dependence of the oscillation amplitude (see Sect. 3.3). In other words, negative Dingle temperature are obtained from the data in Figure 9. More precisely, even though only slightly negative values are obtained for $2a+\delta$ [$T_D = (-1.2 \pm 0.9)$ K], strongly negative T_D's are obtained for $a+\delta$ [$T_D = (-3.2 \pm 1.3)$ K] and $4a+\delta$ [$T_D = (-9 \pm 3)$ K].

Assuming a zero effective cyclotron mass for the b oscillations, the field-dependent part of their amplitude should only depend on R_{MB} (since R_T and R_D are both equal to 1). According to Table 1, equations (1–4) then reduce to $A \propto [1-\exp(-B_0/B)]^2 \exp(-3B_0/B)$ which allows us to determine $B_0 = (41 \pm 9)$ T (see the inset in Fig. 9). This value is only slightly higher than the B_0 value deduced above from the field dependence of the amplitude of the a oscillations and, in any case in agreement with it within the errors bars. In addition, a finite quantum life time τ induces an additional damping factor $R \propto \exp(-\pi m'/eB\tau)$. This damping factor involves a finite effective mass m' which, according to [21], is the sum of the effective masses of the two arms of the interferometer. If neglected, as in the above analysis, this can lead to an apparent increase of the MB field. As a consequence, it can be concluded that the magnetic field and temperature dependence of the b oscillations are consistently accounted for by QI. It must be pointed out that this behaviour is at variance with that of other oscillations such as $a+\delta$ and $4a+\delta$ which put further doubt on the QI origin of these oscillations. Finally, a strong MB-induced damping of the a oscillations at high magnetic field and low temperature is shown in Figure 6a. Solid lines in this figure are fits of equations (1–3) to the data with $B_0 = 33$ T and $T_D = 0.21$ K. Even though a good agreement is observed in the temperature range above ∼1.6 K, strong deviations, that cannot be accounted for by a change of B_0 or T_D, are observed at low temperature even though such deviations are not observed for either the b or the $2a+\delta$ oscillations (see Figs. 6c and 6b, respectively) [23]. In that respect, it should be noticed that oscillations of the chemical potential at very low temperature can significantly influence the oscillatory behaviour. *E.g.*, assuming a fixed number of quasiparticles, the β oscillations in κ-(BEDT-TTF) salts are much more strongly damped, when compared to the fixed chemical potential case, than the α oscillations [8]. A phase transition occurring below 1 K has also been invoked in order to interpret dHvA experiments in (Cl, Cl) [24]. Nevertheless, contrary to the data reported in reference [24], no significant change of the frequency of the oscillations has been observed below 1 K in (Cl, Br).

4 Summary and conclusion

Interlayer magnetoresistance oscillations have been studied in the 2D network of compensated coupled orbits provided by the FS of the organic metal (BEDT-TTF)$_8$Hg$_4$Cl$_{12}$ (C$_6$H$_5$Br)$_2$. The oscillatory spectrum involves more than 15 fundamental frequencies which are linear combinations of the 3 basic frequencies related to the compensated electron and hole orbits (F_a) and of the two FS pieces located in between (F_δ and F_Δ). Among the observed frequency combinations, one of them involving an area equal to the FBZ area ($F_b = 2F_a + F_\delta + F_\Delta$) is consistently accounted for by the LK model, on the basis of QI. In other words, both the magnetic field and the temperature dependencies of the oscillation amplitude are in agreement with a zero effective mass. On the contrary, the LK model fails to consistently account for the data relevant to other frequency combinations. The $2a+\delta$ oscillations, having the highest amplitude after the a oscillations, are certainly due to MB-induced SdH orbits, in agreement with the experimental value of the effective cyclotron mass. The measured value of the low field slope of the Dingle plots (α parameter in Eq. (5)) is nevertheless slightly too small for these oscillations in view of the LK model. Much smaller values of α are derived for the $a+\delta$ and $4a+\delta$ oscillations. Keeping in mind that the data relevant to the b oscillations are in quantitative agreement with QI, the behaviour of $a+\delta$ and $4a+\delta$ strongly suggests that these oscillations are not of QI origin. Instead, they likely result from the oscillation of the chemical potential [8] and (or) the MB-induced broadening of the Landau bands [1]. This latter interpretation certainly holds in the case of *e.g.* the δ oscillation, which has effective cyclotron mass parameter small enough ($m_c = 0.45 \pm 0.10$) to become the dominant oscillation series at temperatures in the range of few K (see Fig. 7) even though both SdH and QI predict much higher m_c values. Simultaneous measurements at high magnetic field of the interlayer magnetoresistance and dHvA effect with high signal-to-noise ratio should clarify this question.

One of the authors (D.V.) would like to acknowledge M. Naughton for his hospitality and precious advice during his stay in Boston. Thanks are also due to J.Y. Fortin, E. Perez, C. Proust, K. Kishigi, T. Ziman and R. Fleckinger for helpful discussions.

References

1. A.B. Pippard, Proc. Roy. Soc. (London) A **270**, 1 (1962)
2. L.M. Falicov, H. Stachowiak, Phys. Rev. **147**, 505 (1966)
3. F.A. Meyer, E. Steep, W. Biberacher, P. Christ, A. Lerf, A.G.M. Jansen, W. Joss, P. Wyder, K. Andres, Europhys. Lett. **32**, 681 (1995)
4. N. Harrison, J. Caulfield, J. Singleton, P.H.P. Reinders, F. Herlach, W. Hayes, M. Kurmoo, P. Day, J. Phys. Cond. Matt. **8**, 5415 (1996)
5. M.V. Kartsovnik, G.Yu. Logvenov, T. Ishiguro, W. Biberacher, H. Anzai, N.D. Kushch, Phys. Rev. Lett. **77**, 2530 (1996)
6. S. Uji, M. Chaparala, S. Hill, P.S. Sandhu, J. Qualls, L. Seger, J.S. Brooks, Synth. Met. **85**, 1573 (1997)

7. E. Steep, L.H. Nguyen, W. Biberacher, H. Müller, A.G.M. Jansen, P. Wyder, Physica B **259-261**, 1079 (1999)
8. K. Kishigi, Y. Hasegawa, Phys. Rev. B **65**, 205405 (2002)
9. P.S. Sandhu, J.H. Kim, J.S. Brooks, Phys. Rev. B **56**, 11566 (1997). J.H. Kim, S.Y. Han, J.S. Brooks, Phys. Rev. B **60**, 3213 (1999). S.Y. Han, J.S. Brooks, J.H. Kim, Phys. Lett. B **85**, 1500 (2000)
10. V.M. Gvozdikov, Yu.V. Pershin, E. Steep, A.G.M. Jansen, P. Wyder, Phys. Rev. B **65**, 165102 (2002)
11. J.W. Eddy, R.W. Stark, Phys. Rev. Lett. **48**, 275 (1982)
12. J.Y. Fortin, T. Ziman, Phys. Rev. Lett. **80**, 3117 (1998)
13. R.N. Lyubovskaia, O.A. Dyachenko, V.V. Gritsenko, Sh.G. Mkoyan, L.O. Atovmyan, R.B. Lyubovskii, V.N. Laukhin, A.V. Zvarykina, A.G. Khomenko, Synth. Metals **41**, 1907 (1991)
14. L.F. Vieros, E. Canadell, J. Phys. I France **4**, 939 (1994)
15. C. Proust, A. Audouard, L. Brossard, S.I. Pesotskii, R.B. Lyubovskii, R.N. Lyubovskaia, Phys. Rev. B **65**, 155106 (2002)
16. M. Nardone, to be published
17. M.J. Naughton, J.P. Ulmet, A. Narjis, S. Askénazy, M.V. Chaparala, A.P. Hope, Rev. Sci. Inst **68**, 4061 (1997); M.J. Naughton, J.P. Ulmet, A. Narjis, S. Askénazy, M.V. Chaparala, R. Richter, Physica B **246**, 125 (1998)
18. R.W. Stark, C.B. Friedberg, Phys. Rev. Lett. **26**, 556 (1971)
19. R.W. Stark, C.B. Friedberg, J. Low Temp. Phys. **14**, 111 (1974)
20. D. Shoenberg, *Magnetic Oscillations in Metals* (Cambridge University Press, Cambridge, 1984)
21. N. Harrison, R.G. Goodrich, J.J. Vuillemin, Z. Fisk, D.G. Rickel, Phys. Rev. Lett. **80**, 4498 (1998)
22. *E.g.*, assuming $m_c = 1.15$, the field dependence of the oscillation amplitude of an orbit involving 4 Bragg reflections at $T = 1.8$ K, computed with the sets of parameters $a_0 = 1$, $T_D = 0.2$ K, $B_1 = 15$ T and $B_2 = 60$ T on the one hand and $a_0 = 0.64$, $T_D = 0.06$ K and $B_1 = B_2 = 35.93$ T on the other hand (a_0 is a prefactor), yield indiscernible data. It is worthwhile to notice that close values of the mean MB field value $B_0 = (B_1 + B_2)/2$ are obtained in both cases
23. Even though solid lines in Figure 6a are obtained with $T_D = 0.21$ K, solid lines in Figure 6b only formally account for the data since, as mentioned in the text, negative T_D values should be used, namely, $T_D = -0.3$ K for $B_0 = 33$ T
24. I.B. Voskoboĭnikov, S.V. Demishev, R.N. Lyubovskaia, V.V. Moschalkov, N.A. Samarin, N.E. Sluchanko, Phys. Sol. State **44**, 210 (2002) [Fiz. Tverdogo Tela **44**, 203 (2002)]